Chemical Engineering Journal 382 (2020) 122858

Contents lists available at ScienceDirect

Chemical Engineering Journal

journal homepage: www.elsevier.com/locate/cej

Promoting opposite diffusion and efficient conversion of polysulfides in “Trap” Fe_xC-Doped asymmetric porous membranes as integrated electrodes

Yang Liu, Xiangcun Li*, Yi Liu, Wei Kou, Weiming Shen, Gaohong He*

State Key Laboratory of Fine Chemicals, Department of Chemical Engineering, Dalian University of Technology, Linggong Road 2#, Dalian 116024, China

HIGHLIGHTS

- Fe_xC dopped porous carbon membranes for integrated Al-free Li-S cathodes.
- Strong adsorption trap polysulfides gradual diffusion into carbon membranes.
- Hierarchical macropores for volume strain and reservoirs of polysulfides.
- Trapping-diffusion-conversion mechanism of polysulfides was proposed.

GRAPHICAL ABSTRACT

Scalable yet flexible Fe_xC/CM membrane with unique triple-layer structure was designed as integrated electrodes for high-performance Li-S batteries. Strong Li-N binding and Fe-S chemical adsorption of Fe_xC induce polysulfides opposite diffusion into macropores as a trap, catalytic effect of Fe_xC further promotes the polysulfides conversion to discharge product (Li_2S/Li_2S_2), realizing smooth trapping-diffusion-conversion process. The dense layer facilitates electrolyte transport instead of traditional Al foil current collector.

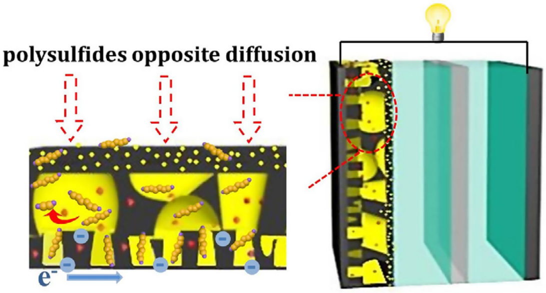

ARTICLE INFO

Keywords:
Lithium-sulfur batteries
Asymmetric porous membrane
Electrocatalysis
Chemical adsorption
Opposite diffusion

ABSTRACT

The shuttling effect in soluble polysulfides results in a sluggish redox reaction and poor cycling performance of Li-S batteries. Herein, a flexible asymmetric porous carbon membrane doped with iron carbide (Fe_xC) nanoparticles was designed by a facile phase-inversion method to serve as an integrated electrode for high-performance Li-S batteries, replacing the traditional Al foil current collector. The strong Li-N binding of the membranes and Fe-S chemical adsorption of Fe_xC can trap polysulfides and promote their gradual diffusion into the porous carbon membrane on the opposite side of the electrolyte. The unique triple-layer-structured multifunctional membrane is ideal as a Li-S battery electrode. The upper spongy-like pores realize physical confinement of polysulfides and sulfur loading; the hierarchical macropores can accommodate volume strain and provide reservoirs for the opposite diffusion of polysulfides; and the dense conductive lower layer can replace Al foil as a current collector. Furthermore, the electrocatalytic effect of Fe_xC on promoting polysulfide conversion and accelerating redox reaction kinetics ensures a smooth trapping-diffusion-conversion mechanism, which greatly suppresses the shuttle effect. The opposite diffusion and catalytic conversion of this flexible membrane is expected to have significant potential for large-scale production in practical applications.

Abbreviations: CM, carbon membrane; PAN, polyacrylonitrile

* Corresponding authors.

E-mail addresses: lixiangcun@dlut.edu.cn (X. Li), hgaohong@dlut.edu.cn (G. He).

https://doi.org/10.1016/j.cej.2019.122858
Received 23 May 2019; Received in revised form 6 August 2019; Accepted 16 September 2019

1. Introduction

The lithium-sulfur (Li-S) battery is attractive for its advantageous high theoretical capacity and energy density as one of the most promising next-generation rechargeable battery systems [1,2]. However, the practical application of Li-S batteries has been hindered by rapid capacity degradation and poor cycle life due to the low conductivity of sulfur and the shuttle effect of soluble polysulfides. Polysulfide intermediates dissolve in organic electrolytes and increase the electrolyte viscosity, leading to blocked electron/ion diffusion and sluggish reaction kinetics [3,4].

Previous efforts have been made to confine polysulfides in cathodes and increase the conductivity of carbon materials serving as sulfur hosts. The structural design of optimized carbon materials includes an appropriate porosity [5,6], conductive framework [7,8], and free-standing electrode [9,10]. However, a nonpolar conductive carbon matrix, with poor adsorption for polar polysulfides, results in rapid capacity decay and diffusion of polysulfides to the electrolyte. Moreover, the weak coverage of intermediate polysulfides on carbon materials and the high nucleation barrier of Li_2S result in an inferior reaction conversion. To address the "shuttle effect," the stronger chemical adsorption abilities of polar metal oxides such as TiO_2 [11], Ti_4O_7 [12,13], Co_3O_4 [14], and CeO_2 [15] have been widely investigated as an efficient strategy to block polysulfide shuttling; the designed structures can function as polysulfide immobilizers by both physical and chemical trapping. Unfortunately, the intrinsically poor electrical conductivity restricts electron transfer, resulting in failed surface conversion on the polar host and excess polysulfides remaining on the surface. Saturation sites are an inevitable consequence of slow redox reaction kinetics and polysulfide diffusion with diminishing performance. Thus, the main factors for electrochemical kinetics are a sufficient adsorption affinity and efficient charge transfer. Compared with the weak adsorption of nonpolar carbon materials and poor conductivity of metal oxides, metallic materials such as metal carbides [16,17], metal nitrides [18–20], and metal phosphides [21] can accelerate the transformation of soluble polysulfides by providing adequate binding sites and fast charge transport. This simultaneously meets the demands for sufficient surface binding and the surface diffusion step, as shown in Fig. 1a.

Herein, we designed an iron carbide (Fe_xC)-nanoparticle-doped flexible asymmetric porous carbon membrane for Al-free high-capacity Li-S batteries, in which physical confinement, chemical adsorption, and electrocatalysis of polysulfide conversion to final discharge products were successfully realized, as shown in Fig. 1b. These factors prevent polysulfides from diffusing into the electrolyte and lessen the shuttle effect compared with the control pure C membrane (CM) and Al cathode (Fig. 1c and d). The Fe_xC asymmetric porous carbon membrane was employed to entrap S and has the following merits: (1) the abundantly porous structure can accommodate volume expansion during charge/discharge and provide reservoirs for the opposite diffusion of polysulfides; (2) fast pathways for ion/electron transport improve the reaction kinetics and rate performance; (3) effectively suppresses polysulfide shuttling by physically blocking sponge-like pores and by the chemical affinity of the Fe_xC nanoparticles.

Furthermore, the double functionality of Fe_xC can not only effectively capture intermediate polysulfides via strong adsorption by Fe-S bonding, but also effectively promote entrapped polysulfide redox kinetics and fast electron transfer as a catalyst [22]. The unique Fe_xC-doped porous carbon membrane (Fe_xC/CM) exhibits an excellent cycling stability and high Coulombic efficiency by realizing a fast trapping-diffusion-conversion mechanism of intermediate polysulfides.

2. Experimental section

2.1. Synthesis of fine Fe_2O_3 nanoparticles

Nanosized Fe_2O_3 particles were prepared by mixing of 60 ml of 0.018 M $FeCl_3{\cdot}6H_2O$ and 0.01 M HCl solutions, referring to a microwave hydrothermal method [23]. The mixture was treated at 160 °C under 300 W microwave for 1 h. After washing the precipitate by deionized distilled water and ethanol three times, the obtained collection was dried at 60 °C overnight.

2.2. Preparation of CM and Fe_xC/CM membranes

The Fe_xC/CM membrane was prepared by a facile phase inversion method. The casting solution was an *N,N*-dimethylformamide (Aladdin, > 99.9%) homogenous suspension composed of 20% aforementioned fine Fe_2O_3 nanoparticles and 15 wt% polyacrylonitrile (PAN, MW = 40000, Aladdin, > 99%) after magnetic stirring for 2 h at 80 °C in an oil bath. The mixture was allowed to stand overnight to remove internal bubbles, then casted onto a glass plate at a thickness of ~150 μm by an automatic scraping knife; the thickness was optimized by adjusting the scraping knife. Subsequently, the precursor-solution-coated glass plate was rapidly immersed into deionized water for solvent exchange and phase inversion to form a Fe_2O_3/PAN asymmetric porous membrane. The obtained red Fe_2O_3/PAN membrane was dried at 90 °C in a vacuum oven, then heated at 250 °C in air for preoxidation to enhance the mechanical strength. Finally, the composite membrane was further carbonized in an argon gas atmosphere at 700 °C for 1 h at a heating rate of 5 °C min^{-1} to obtain the Fe_xC/CM membrane. A pure CM membrane was also prepared in the same way without adding Fe_2O_3 during the preparation of the casting solution. The as-prepared CM and Fe_xC/CM membranes were cut into circular discs with a diameter of 14 mm (1.5 cm^{-2}) to prepare the electrodes.

2.3. S loading on Fe_xC/CM and CM membrane electrodes

A C/S hybrid was prepared with carbon black and sulfur powder at a mass ratio of 1:2 and heated at 155 °C for 12 h in argon by a melt-diffusion method. Then, 90 mg of the obtained C/S hybrid was mixed with 10 mg of polyvinylidene fluoride binder dissolved in 600 μl of *N*-methyl pyrrolidone to form a C/S electrode slurry. The slurry was uniformly coated on the sponge-like porous surface of the Fe_xC/CM membrane, CM membrane, and Al foil with S loading of ~1.5 mg/cm^2. The E/S ratios were 21, 12 and 7 μl/mg for Li-S batteries for sulfur mass loadings of ~1.5, 2.7, and ~4.6 mg/cm^2, respectively, in this work.

2.4. Adsorption test

Li_2S and sulfur with a molar ratio of 1:5 were added into a 1,3-dioxolane/1,2-dimethoxyethane mixture (1:1, v/v) and stirred in an argon-filled glove box to obtain a 0.1 M Li_2S_6 solution. The Li_2S_6 solution (100 μl) was dissolved in 20 ml of electrolyte to form a diluted solution. Then, 20 mg of super P, CM, and Fe_xC/CM materials were added to 4 ml of the mixture solution and allowed to stand for 24 h for observation.

2.5. Characterization

The morphology and energy-dispersive X-ray spectroscopic (EDX) element mappings were monitored by scanning electron microscopy (Nova Nano SEM 450), and crystal phases were characterized by X-ray diffraction (XRD, D/MAX-2400 diffractometer, Cu Kα radiation, 0.154 nm). The S content was analyzed by thermogravimetric analysis (TA Instruments Q50 TGA), and the interaction between Fe_xC and polysulfides was tested by using X-ray photoelectron spectroscopy (XPS, ESCALAB 250 Xi).

2.6. Computational methods

All calculations were carried out using the $DMOL_3$ package based on density functional theory (DFT). The double numerical plus

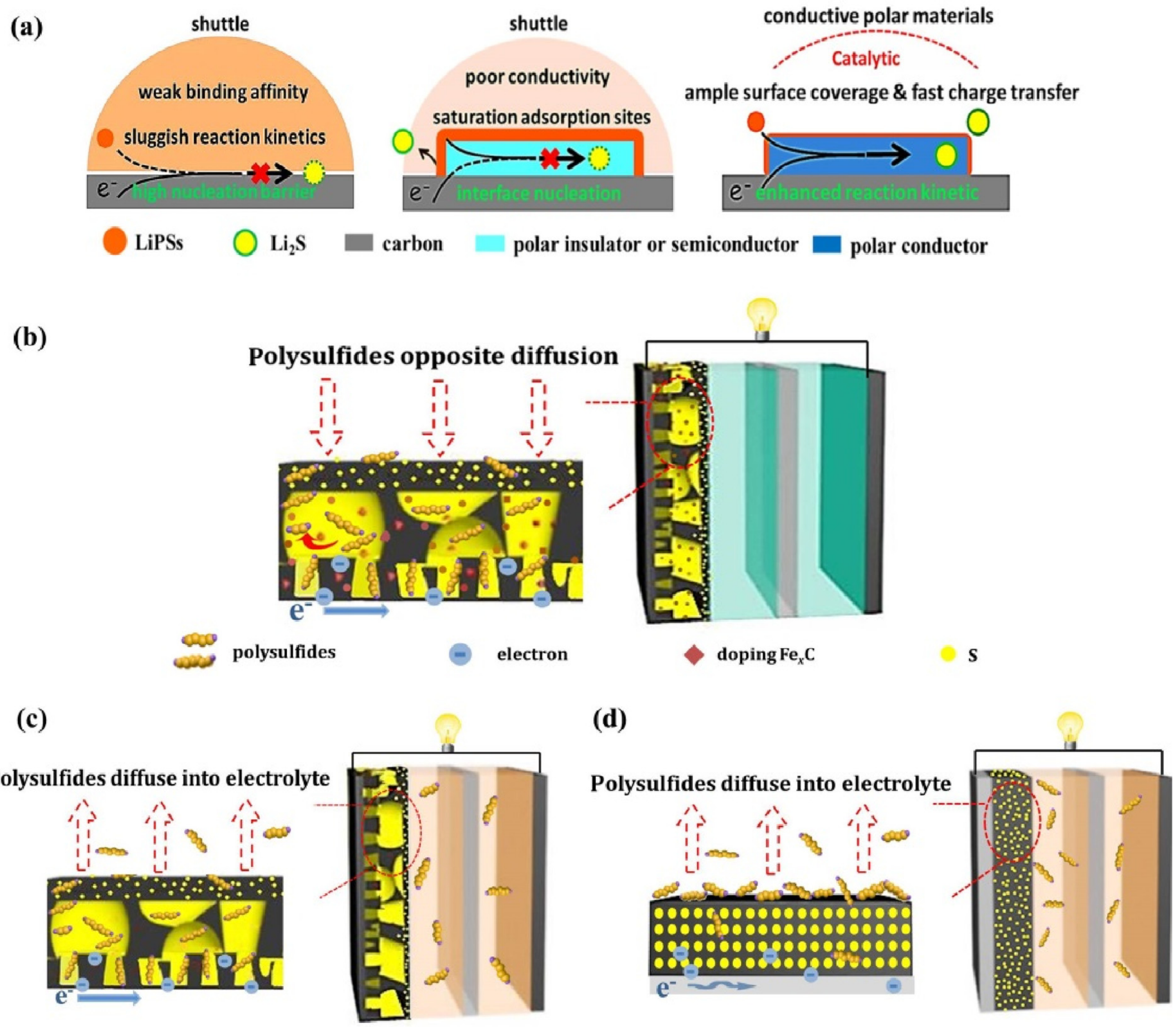

Fig. 1. (a) Illustration of fast reaction kinetics of polysulfides on polar conductor based on the adsorption and conversion mechanism for different hosts; (b) schematic of Fe_xC/CM as integrated electrodes promoting the opposite diffusion of polysulfides with fast electron transfer; (c) polysulfide diffusion into electrolyte from pure CM without the adsorption effect of Fe_xC; (d) polysulfide diffusion into electrolyte from traditional Al-free cathode with impeded transfer.

polarization function (DNP basis set) and generalized gradient approximation with the Perdew–Burke–Ernzerhof exchange-correlation functional were used to optimize geometrical structures and calculate energies. The vacuum layer was set to ~8 Å to eliminate slab interactions in the z-direction. Convergence was achieved when energy, force, and maximum displacement reached a minimum of 2×10^{-5} Ha, 0.004 Ha Å^{-1}, and 0.005 Å, respectively. To simplify the modeling, Fe_4C was chosen to replace Fe_xC, and the adsorption energy was defined as: $E_{ads} = E(\text{polysulfide}/Fe_4C) - E(\text{polysulfide}) - E(Fe_4C)$, where E (polysulfide/Fe_4C) is the total energy of the Fe_4C (2 2 0) surface with polysulfide, E(polysulfide) is the energy of the polysulfide, and $E(Fe_4C)$ is the energy of the (2 2 0) surface of Fe_4C.

2.7. Electrochemical measurements

The electrochemical properties of the Fe_xC/CM and CM membranes were evaluated by CR2025 coin-type cells directly assembled in an argon-filled glove box. The cells consisted of metal lithium, polypropylene/polyethylene/polypropylene membranes (Celgard) as separators, and the S-loaded Fe_xC/CM and CM membranes as cathodes. A nonaqueous solution (1:1, 1,2-dimethoxyethane and 1,3-dioxolane) with 1 M LiTFSI was used as the electrolyte. The cycling performance and charge–discharge current from rate capability tests were measured by using a LAND CT2001A multichannel battery test system with a voltage range of 1.7 to 2.8 V (vs Li/Li^+). Cyclic voltammetry (CV) curves at a scan rate of 0.05 mV s^{-1} and electrochemical impedance spectroscopy (EIS) measurements with a frequency range of 100 kHz–0.01 Hz were performed on an Ivium Powerstat (Ivium Technologies, the Netherlands) electrochemical workstation.

3. Results and discussion

The preparation of Fe_xC/CM- and CM-integrated S-host materials via phase inversion is shown in Fig. 2a. Fine Fe_2O_3 nanoparticles were produced by a microwave hydrothermal method (Fig. S1); the sufficiently fine size of dozens of nanometers ensured a uniform Fe_2O_3 distribution. The red casting membrane solution (Fig. 2b) was tiled onto a glass plate at a thickness of 150 μm by automatic membrane casting equipment. Fig. 2c and d show the phase transformation process and large-scale production of the Fe_2O_3/PAN asymmetric membranes, and Fig. 2e shows the transformation of the membrane from red to black after preoxidation and carbonization. The XRD pattern in Fig. S2a verified the existence of Fe in $Fe_{1.88}C_{0.12}$ and Fe_2C states in the asymmetric porous membrane (JCPDS 44-1293, JCPDS 44-1293); the Fe_xC content was approximately 23% as calculated by TGA, as shown in Fig. S2b. The designed membrane is flexible (Fig. S3j) enough to cut into

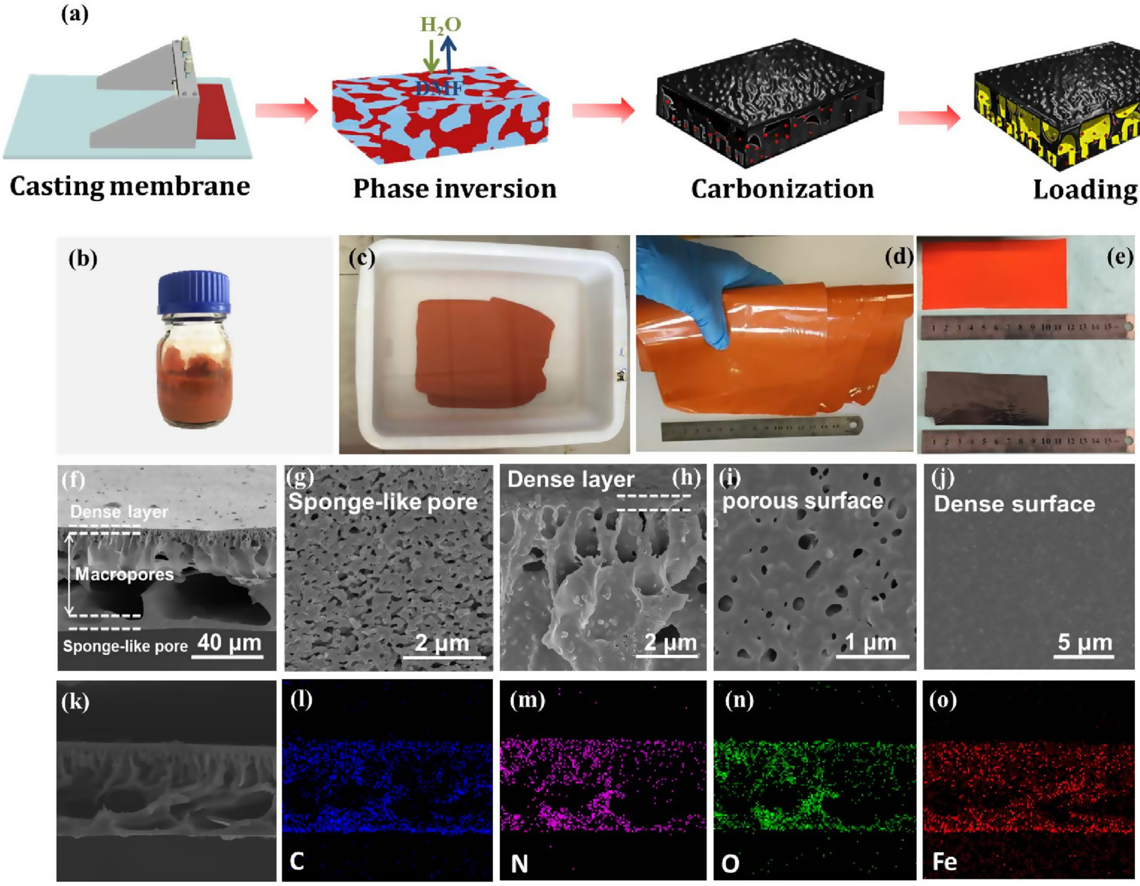

Fig. 2. (a) Schematic of preparation of Fe_xC/CM membrane; (b) photo of membrane casting solution with Fe_2O_3 nanoparticles; (c) solvent exchange process between DMF and deionized water accompanied by pore formation; (d) photo of Fe_2O_3/PAN membrane; (e) photo of Fe_2O_3/PAN membrane compared with its carbonization into Fe_xC/CM membrane; (f-h) cross-sectional SEM images of Fe_xC/CM membrane; (i-j) surfaces of the Fe_xC/CM membrane; (k-o) EDX elemental mapping images of Fe_xC/CM membrane.

circular shapes for electrode fabrication (Fig. S3e). The asymmetric porous structure (shown in Fig. 2f-j) generated during the phase inversion process as a result of different exchange rates, rapid nonsolvent diffusion, and polymer precipitation opposite the glass plate resulted in the generation of a dense layer, and an inner polymer-poor layer formed with continuous macropores. Near the plate glass, the impeded diffusion process tended to form sponge-like pores. As a comparison, SEM images of CM and the preoxidized Fe_xC/CM are also shown in Fig. S3; the membrane with Fe_2O_3 shows a hierarchical porous structure in the polymer framework. N_2 adsorption analysis of the Fe_xC/CM membranes (Fig. S4) indicated a specific surface area of 54.479 $m^2\ g^{-1}$, with the average size of mesoporous of 3.9 nm ascribed to honeycomb-like pores, indicating the porous features of the Fe_xC/CM membrane and its superiority for rapid diffusion of electrolyte and ions. The EDX elemental mappings (Fig. 2k–o) confirmed the uniform distributions of C, N, O, and Fe elements in the asymmetric porous membrane structure.

The polar metal carbides commonly used in Li-S batteries not only suppress the shuttling effect via the strong chemical adsorption of polysulfides but also have electrochemical catalytic activity for the conversion of polysulfides by accelerating electron conduction. XPS was employed to understand the interaction between Fe_xC/CM and polysulfides after cycling. The XPS S 2p peaks are displayed in Fig. 3a and b. The S 2p peaks between 166 and 172 eV were attributed to thiosulfate and polythionate species; the peaks at approximately 165 and 164 eV were due to S $2p_{3/2}$ (C-S-C) and S $2p_{1/2}$ (C-S-C) bonds, respectively [24,25]; and the peaks at 160.2 and 161.7 eV corresponded to Li_2S and Li_2S_2 in discharged states, respectively. The intensive peak areas of Fe_xC/CM in the S 2p spectrum indicated complete conversion of long-chain polysulfides to short-chain polysulfides, demonstrating the enhancement of the polysulfide conversion reaction kinetics [26,27]. Moreover, the immobilization ability toward polysulfides can be proved by the peak at 162.6 eV from Fe-S bonds in the S 2p spectrum. In Fig. 3c, the Fe 2p peak located at 708.8 eV from Fe-S bonds also verified the strong chemical adsorption interaction between Fe_xC and sulfur species [28]. The DFT calculation results in Fig. 3d show that the adsorption energies (E_{ads}) of Li_2S, Li_2S_4, and Li_2S_6 on the Fe_xC (2 2 0) surface were −3.12, −4.54, and −6.46 eV respectively, which further revealed the strong binding interactions between Fe_xC and polar polysulfides. The XPS of the Fe_xC/CM materials also clearly proved the existence of C, N, and Fe elements as shown in Fig. S5a–c. The N 1s spectrum can be split into peaks with binding energies of 398.1 and 400.2 eV corresponding to pyridinic N and pyrrolic N, respectively. These doped N atoms in the carbon membrane increase the polarity, which can enhance the adsorption of polysulfides [29]. The binding energies experienced positive shifts of +0.1 eV (400.3 eV, pyridinic N) and +0.7 eV (398.7 eV, pyrrolic N) after cycling of Fe_xC/CM as the sulfur host material, arising from Li-N bonds with a strong affinity between doped N and polysulfides [30]. The UV–Vis spectra in Fig. S6 further indicated the adsorption capability and polysulfide opposite diffusion of the membrane. The peak intensity at approximately 250–300 nm can be attributed to Li_2S_6 species [31,32], and the weaker absorption band of Fe_xC/CM indicates that less lithium polysulfides are dissolved into the electrolyte. In Fig. 3e, a digital image shows the visible decoloration of the Li_2S_6 solution after the strong adsorption, also demonstrating that the Li_2S_6 species diffuse from the electrolyte into the Fe_xC/CM membrane.

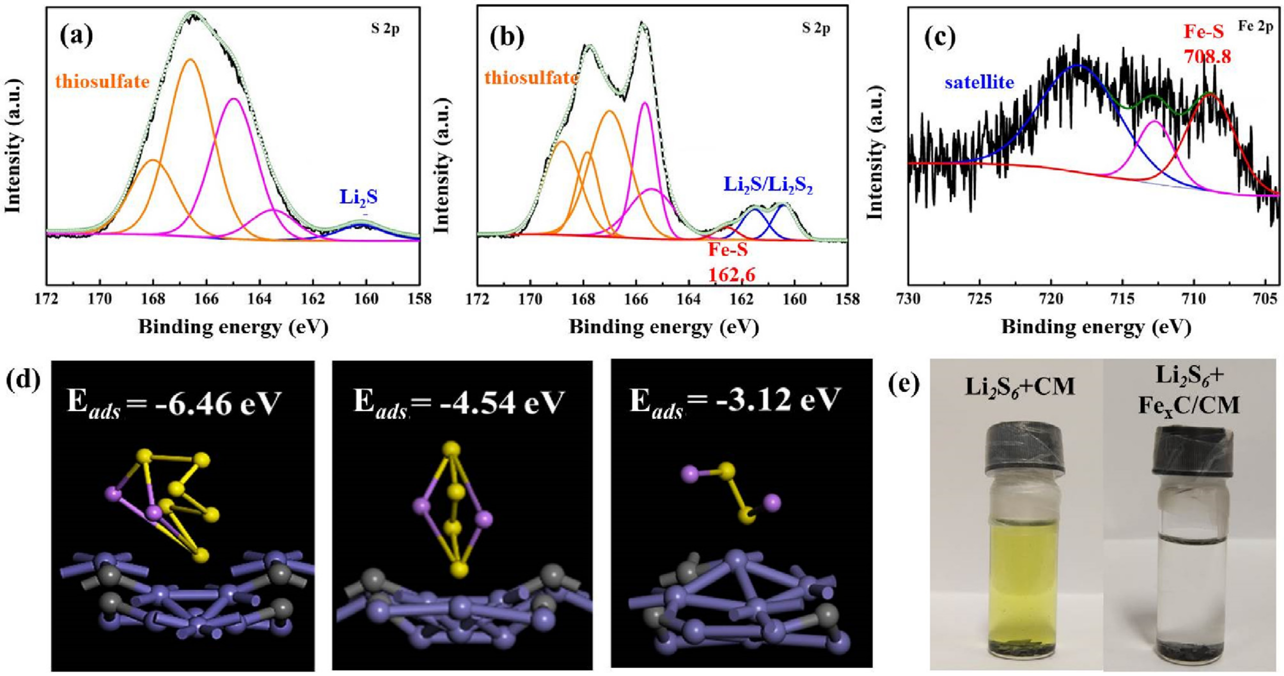

Fig. 3. (a) XPS S 2p spectrum of CM membrane; (b) S 2p spectrum of Fe_xC/CM membrane; (c) Fe 2p spectrum of Fe_xC/CM membrane as cathode in discharged state; (d) interactions between Fe_xC and polysulfides, theoretical calculations based on DFT; (e) adsorption ability tests of Fe_xC/CM and CM membranes with Li_2S_6.

The lithium ion diffusion coefficient (D_{Li+}) is a criterion for testing the promotion of polysulfide redox reaction kinetics. CV at different scan rates was employed to investigate the immobilization of polysulfide species and electrode kinetics in relation to D_{Li+}. Fig. S7a and b show the CV curves of Fe_xC/CM and CM. The two cathodic peaks at approximately 2.26 V (denoted Ic_1) and 1.92 V (denoted Ic_2) at a scanning rate of 0.1 mV/s for Fe_xC/CM (1.90 and 2.23 V for CM) result from the reduction of S_8 to long-chain polysulfides and subsequent transformation to short-chain polysulfides. The anodic peak at approximately 2.47 V for Fe_xC/CM and 2.46 V for CM in the anodic sweep (denoted I_a) is related to the oxidation of short-chain polysulfides to long-chain polysulfides and sulfur. The value of D_{Li+} is the slope of the peak current (I_P) versus the square root of the scan rate ($V^{0.5}$) in Fig. S7c-e based on the Randles–Sevcik equation as follows [21,28]:

$$I_P = 2.69 \times 10^5 n^{1.5} A D_{Li^+}^{0.5} C_{Li^+} \nu^{0.5}$$

where I_P is the peak current; n is the number of transferred electrons, which is 2 for Li-S cells; A is the electrode geometric area, which is 1.54 cm^2; $C_{Li}{}^+$ is the Li ion concentration change during the electrochemical reaction; and ν is the scan rate. The calculated diffusion coefficients with different scan rates varying from 0.03 to 0.2 $mV\,s^{-1}$ for Fe_xC/CM at peaks Ic_1, Ic_2, and I_a are 1.04×10^{-8}, 2.51×10^{-8}, and 4.11×10^{-8} $cm^2\,s^{-1}$, respectively (Table 1), which are higher than those of CM (0.72×10^{-8}, 1.08×10^{-8}, and 3.22×10^{-8} $cm^2\,s^{-1}$); this faster diffusion indicates enhanced reaction kinetics on the Fe_xC/CM electrode. It is known that intermediate products dissolve easily in the electrolyte, leading to a series of problems such as the shuttle effect, an increase in electrolyte viscosity, and poor electroconductivity, thereby hindering lithium ion diffusion. Fe_xC offers sufficient sites for both the adsorption and conversion of polysulfides with the large surface of the carbon membrane, thus promoting fast lithium ion diffusion. EIS measurements also confirmed the enhanced redox kinetics. In Figs. S7f and S8, the diameter of the low-frequency semicircle represents the charge transfer resistance (R_{ct}). The Fe_xC/CM electrode had a lower R_{ct} both before and after cycling, reflecting the facile charge transfer resulting from the higher conductivity of Fe_xC and stronger affinity for polysulfides [33].

Table 1
Li-ion diffusion coefficients ($cm^2\,s^{-1}$) of Fe_xC/CM, CM, and other reported materials.

Sample	Ic_1	Ic_2	I_a
Fe_xC/CM	1.04×10^{-8}	2.51×10^{-8}	4.11×10^{-8}
CM	0.72×10^{-8}	1.08×10^{-8}	3.22×10^{-8}
CNFs/MnO_2 [34]	4.83×10^{-9}	7.24×10^{-9}	2.04×10^{-8}
Ni-ZIF-8@CC [35]	3.67×10^{-8}	8.01×10^{-8}	1.39×10^{-7}
SWCNT modulated separators [36]	1.07×10^{-8}	1.18×10^{-8}	1.79×10^{-8}

The electrochemical performance of the Fe_xC/CM membrane electrode for Li-S batteries was investigated. Fig. 4a displays the typical CV profiles of the sulfur-loaded Fe_xC/CM and CM membrane electrodes at a scan rate of 0.1 $mV\,s^{-1}$. The intensities of the reductive peaks at 2.02 and 2.29 V were higher for Fe_xC/CM, indicating a greatly enhanced reaction. Fig. 4b shows the charge/discharge curves of the Fe_xC/CM and CM cathodes at 0.1C; the longer plateaus at approximately 2.1 V suggest promotion of the transformation of long-chain polysulfides to short-chain polysulfides. It was noted that the Fe_xC/CM cathode showed a lower overpotential of 161 mV compared with CM, which reveals that the introduction of Fe_xC greatly enhances the reduction efficiency of polysulfides and reduces the polarization. Fig. S9 shows the charge/discharge curves of the Fe_xC/CM and CM cathodes at different current densities, further confirming the enhanced redox reaction kinetics. Fe_xC/CM yielded an initial discharge capacity of 949.9 $mAh\,g^{-1}$, which decreased to 829.1 $mA\,h\,g^{-1}$ after 100 cycles with a coulombic efficiency of 99.4% at 0.2C as shown in Fig. 4c (0.13% decay per cycle). On the other hand, the CM and traditional Al foil electrodes exhibited only 658.6 $mA\,h\,g^{-1}$ (0.18% decay per cycle) and 471.1 $mA\,h\,g^{-1}$ (0.45% decay per cycle) at 0.2C after 100 cycles (Fig. S10a). At a current density of 1C, Fe_xC/CM delivered 610.8 $mA\,h\,g^{-1}$ at 1 C after 350 cycles with a capacity decay rate of 0.11% per cycle, as shown in Fig. 4d. In contrast, the CM and traditional Al foil electrodes rapidly decreased to 525.8 $mA\,h\,g^{-1}$ and 384.8 $mA\,h\,g^{-1}$ at 1C with higher capacity decay rates of 0.36% and 0.66% per cycle, respectively. The rate capabilities of the Fe_xC/CM cathode, CM cathode, and Al foil electrode are evaluated in Fig. 4e and Fig. S10b. The Fe_xC/CM cathode showed discharge capacities of

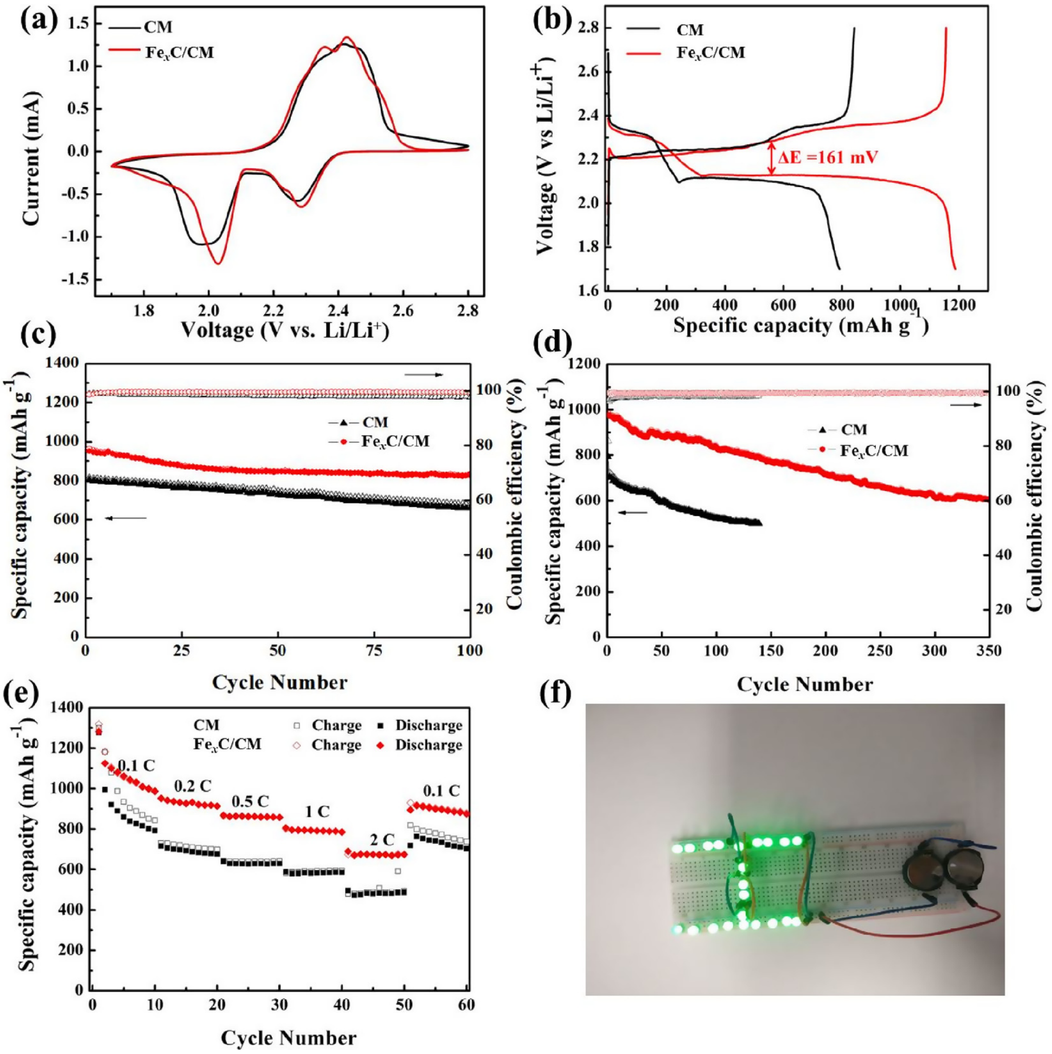

Fig. 4. (a) CV curves of Fe_xC/CM and CM membrane electrodes in voltage range of 1.7–2.8 V at a scan rate of 0.1 mV s^{-1}; (b) typical charge-discharge curves of Fe_xC/CM and CM membrane electrodes at 0.1 C; (c-d) cycling performance of Fe_xC/CM and CM membrane cathodes at 0.2 and 1.0 C, respectively; (e) rate performance of Fe_xC/CM and CM membrane cathodes; (f) an LED lamp lit by two Fe_xC/CM membrane electrode cells, suggesting its practical applications.

1105.9, 985.8, 864.6, 800.9, and 674.5 mA h g^{-1} with increasing current densities of 0.1, 0.2, 0.5, 1, and 2 C, respectively, which are higher than those of the CM cathode and Al cathode. The E/S ratio is an important indicator for Li-S batteries. Low the E/S ratio can suppress polysulfides disproportionation and achieve a high specific capacity. To meet the needs of Li-S battery in practical applications, the higher sulfur mass loading of Fe_xC/CM electrodes were measured. As shown in Fig. S11, the areal capacity of 1.7 and 2.6 mAh cm^{-2} at 0.2 C after 100 cycles with the sulfur loading of 2.7 mg/cm^2 and 4.6 mg/cm^2 respectively. As shown in Fig. 4f, green light-emitting diodes were lit with two Fe_xC/CM cells, suggesting that their good stability and fast kinetics have great promise for future commercial applications.

The excellent performance of the Li-S batteries based on the Fe_xC/CM composite can be ascribed to the following aspects. First, a scalable and flexible carbon membrane was used as an integrated electrode instead of the traditional Al current collector; the macropores accelerate ion transfer and are conducive to a high conductivity, while the porous structure provides sufficient space for polysulfide storage and volume expansion. Then, strong adsorption resulting from Fe-S bonds between polar Fe_xC and Li-N results in the affinity of the carbon membrane for polysulfides, which can offer sufficient surface sites to draw polysulfides into diffusing into the carbon membrane as a trap, as shown in Fig. 5a. During the charge-discharge process, the soluble polysulfides gradually move to the carbon membrane via the strong affinity of Fe_xC. The Fe_xC/CM cathode realizes direct induction and rapid opposite diffusion of polysulfides, then achieves efficient conversion based on a trapping-diffusion-conversion mechanism. The gradual polysulfide diffusion process into the membrane can be verified by the EDS of the electrodes before cycling (Fig. 5c1–g1), after a few cycles (Fig. 5c2–g2), and after hundreds of cycles (Fig. 5c3–g3). The strong polysulfide-capturing capability of polar Fe_xC is crucial for inducing the opposite diffusion of polysulfides and realizing faster polysulfide conversion kinetics. Otherwise, a great deal of polysulfides would easily diffuse into the electrolyte from the carbon substrate, resulting in the shuttle effect and uncontrollable deposition of Li_2S. The opposite diffusion can be further confirmed by the optical images of traditional Al current collector electrodes and separators and those in the Fe_xC/CM and CM batteries after cycling at 1 C, as shown in Fig. 5b. Compared with the lithium plates and separators of the traditional Al and CM batteries, Fe_xC/CM was a lighter yellow, indicating the lowest amount of residual polysulfides on the separator and lithium plates. This is direct evidence that the soluble polysulfides in the electrolyte diffuse to the electrodes oppositely owing to the strong Li-N binding of the membranes and Fe-S chemical adsorption of Fe_xC. Last but most importantly, Fe_xC can serve as a catalyst to enable fast polysulfide conversion and accelerate the polysulfide redox reaction kinetics for the enhanced performance of Li-

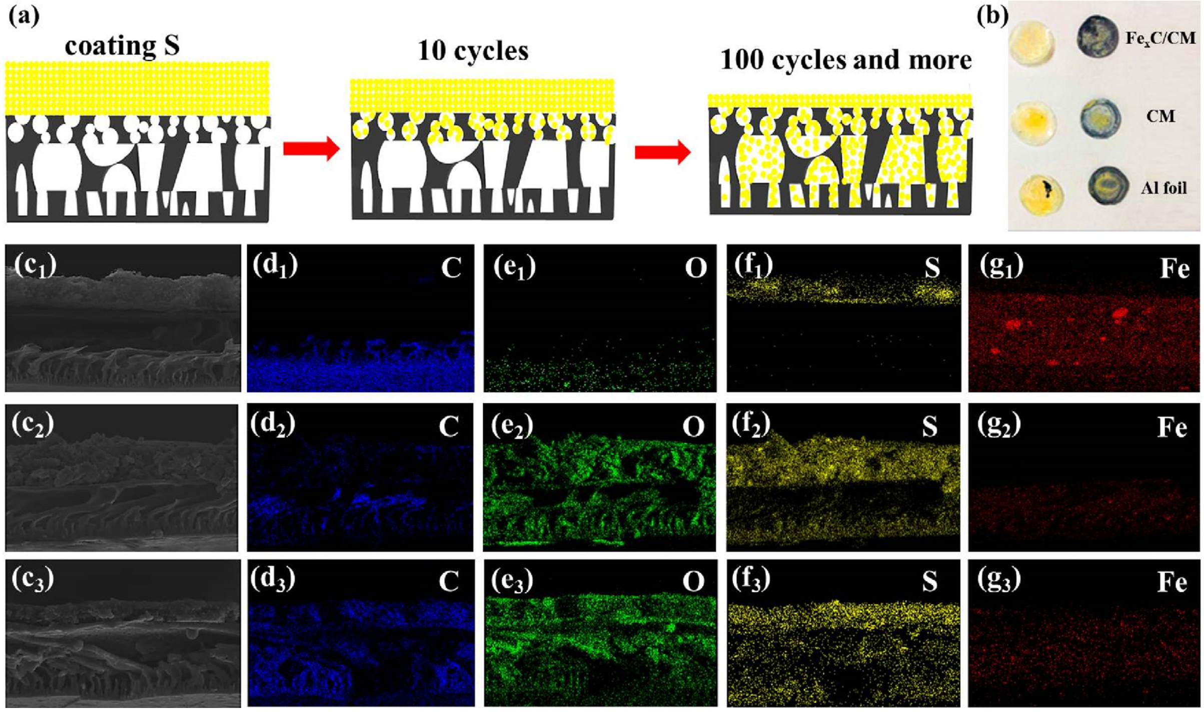

Fig. 5. (a) Schematic of Fe$_x$C/CM membrane promoting the gradual immersion of polysulfides by the strong trapping of Fe$_x$C during the charge-discharge process; (b) Optical photos of lithium plates and separators from traditional Al foil battery and from Fe$_x$C/CM and CM batteries after cycling; EDX element mapping images of the (c$_1$-g$_1$) Fe$_x$C/CM cathode before cycling, (c$_2$-g$_2$) Fe$_x$C/CM cathode after a few cycles, and (c$_3$-g$_3$) Fe$_x$C/CM cathode after hundreds of cycles.

S batteries.

4. Conclusions

In summary, we have proposed a novel Fe$_x$C-doped asymmetric porous carbon membrane as a current collector instead of traditional Al foil in Li-S batteries to trap and promote polysulfide opposite diffusion, as well as to further facilitate their conversion to discharge products. XPS measurements verified that the strong adsorption of Fe$_x$C/CM by Fe-S and Li-N binding can serve as adsorption sites to trap polysulfides and promote polysulfide opposite diffusion, which agreed with the corresponding DFT calculations. Fe$_x$C further promotes polysulfide conversion reactions and reduces the Li_2S nucleation energy, thus meeting the demands for both sufficient adsorption sites and efficient electron transfer. The beneficial electrocatalytic activities of Fe$_x$C that promote the redox reactions of polysulfide conversion were revealed by electrochemical analytical techniques (EIS and CV curves) and the XPS S 2p spectrum. In this manner, the polysulfide shuttle effect is largely suppressed, and the redox reaction kinetics are significantly improved. Accordingly, the Fe$_x$C/CM cathode delivers an excellent discharge capacity of 833.7 $\mathrm{mA\,h\,g^{-1}}$ at 0.2C after 100 cycles and 610.8 $\mathrm{mA\,h\,g^{-1}}$ at 1 C after 350 cycles with a capacity decay rate of 0.11% per cycle. Considering the demonstrated simple preparation process and dual merits of adsorption and catalysis, this work offers a new strategy to achieve smooth trapping-diffusion-conversion of polysulfides for large-scale processes toward high-performance Li-S batteries.

Declaration of Competing Interest

The authors declare that they have no known competing financial interests or personal relationships that could have appeared to influence the work reported in this paper.

Acknowledgements

Financial support from the Natural Science Foundation of China [grant numbers 21476044, 21676043], Fundamental Research Funds for the Central Universities and Dalian [grant number DUT15QY08, 2019J12SN68], and Changjiang Scholars Program [grant number T2012049] are greatly appreciated.

Appendix A. Supplementary data

Supplementary data to this article can be found online at https://doi.org/10.1016/j.cej.2019.122858.

References

[1] L.F. Nazar, M. Cuisinier, Q. Pang, Lithium-sulfur batteries, MRS Bull. 39 (2014) 436–442.
[2] A. Manthiram, S.H. Chung, C. Zu, Lithium-sulfur batteries: progress and prospects, Adv. Mater. 27 (2015) 1980–2006.
[3] Y. Qiu, W. Li, G. Li, Y. Hou, L. Zhou, H. Li, M. Liu, F. Ye, X. Yang, Y. Zhang, Polyaniline-modified cetyltrimethylammonium bromide-graphene oxide-sulfur nanocomposites with enhanced performance for lithium-sulfur batteries, Nano Res. 7 (2014) 1355–1363.
[4] R. Singhal, S.H. Chung, A. Manthiram, V. Kalra, A free-standing carbon nanofiber interlayer for high-performance lithium-sulfur batteries, J. Mater. Chem. A 3 (2015) 4530–4538.
[5] N. Moreno, A. Caballero, L. Hernan, J. Morales, J. Canales-Vazquez, Ordered mesoporous carbons obtained by a simple soft template method as sulfur immobilizers for lithium-sulfur cells, Phys. Chem. Chem. Phys. 16 (2014) 17332–17340.
[6] G. He, S. Evers, X. Liang, M. Cuisinier, A. Garsuch, L.F. Nazar, Tailoring porosity in carbon nanospheres for lithium-sulfur battery cathodes, ACS Nano 7 (2013) 10920–10930.
[7] S. Lu, Y. Chen, X. Wu, Z. Wang, Y. Li, Three-dimensional sulfur/graphene multifunctional hybrid sponges for lithium-sulfur batteries with large areal mass loading, Sci. Rep. 4 (2014) 4629–4632.
[8] Y. Fang, Y. Lv, R. Che, H. Wu, X. Zhang, D. Gu, G. Zheng, D. Zhao, Two-dimensional mesoporous carbon nanosheets and their derived graphene nanosheets: synthesis and efficient lithium ion storage, J. Am. Chem. Soc. 135 (2013) 1524–1530.
[9] G. Zhou, L. Li, C. Ma, S. Wang, Y. Shi, N. Koratkar, W. Ren, F. Li, H.M. Cheng, A graphene foam electrode with high sulfur loading for flexible and high-energy Li–S batteries, Nano Energy 11 (2015) 356–365.
[10] G. Zhou, S. Pei, L. Li, D.W. Wang, S. Wang, K. Huang, L.C. Yin, F. Li, H.M. Cheng, A

graphene-pure-sulfur sandwich structure for ultrafast, long-life lithium-sulfur batteries, Adv. Mater. 26 (2014) 625–631.
[11] Z.W. Seh, W. Li, J.J. Cha, G. Zheng, Y. Yang, M.T. McDowell, P.C. Hsu, Y. Cui, Sulphur-TiO_2 yolk-shell nanoarchitecture with internal void space for long-cycle lithium-sulphur batteries, Nat. Commun. 4 (2013) 1331–1336.
[12] Q. Pang, D. Kundu, M. Cuisinier, L.F. Nazar, Surface-enhanced redox chemistry of polysulphides on a metallic and polar host for lithium-sulphur batteries, Nat. Commun. 5 (2014) 4759–4766.
[13] X. Tao, J. Wang, Z. Ying, Q. Cai, G. Zheng, Y. Gan, H. Huang, Y. Xia, C. Liang, W. Zhang, Y. Cui, Strong sulfur binding with conducting Magnéli-phase $Ti_{(n)}O_{2(n-1)}$ nanomaterials for improving lithium-sulfur batteries, Nano Lett. 14 (2014) 5288–5294.
[14] F. Ma, J. Liang, T. Wang, X. Chen, Y. Fan, B. Hultman, H. Xie, J. Han, G. Wu, Q. Li, Efficient entrapment and catalytic conversion of lithium polysulfides on hollow metal oxide submicro-spheres as lithium-sulfur battery cathodes, Nanoscale 10 (2018) 5634–5641.
[15] L. Ma, R. Chen, G. Zhu, Y. Hu, Y. Wang, T. Chen, J. Liu, Z. Jin, Cerium oxide nanocrystal embedded bimodal micro-mesoporous nitrogen-rich carbon nanospheres as effective sulfur host for lithium-sulfur batteries, ACS Nano 11 (2017) 7274–7283.
[16] H.J. Peng, G. Zhang, X. Chen, Z.W. Zhang, W.T. Xu, J.Q. Huang, Q. Zhang, Enhanced electrochemical kinetics on conductive polar mediators for lithium-sulfur batteries, Angew. Chem. Int. Ed. 128 (2016) 13184–13189.
[17] F. Zhou, Z. Li, X. Luo, T. Wu, B. Jiang, L.L. Lu, H.B. Yao, M. Antonietti, S.H. Yu, Low cost metal carbide nanocrystals as binding and electrocatalytic sites for high performance Li-S batteries, Nano Lett. 18 (2018) 1035–1043.
[18] D.R. Deng, F. Xue, Y.J. Jia, J.C. Ye, C.D. Bai, M.S. Zheng, Q.F. Dong, Co_4N nanosheets assembled mesoporous sphere as a matrix for ultrahigh sulfur content lithium-sulfur batteries, ACS Nano 11 (2017) 6031–6039.
[19] L. Zhang, X. Chen, F. Wan, Z. Niu, Y. Wang, Q. Zhang, J. Chen, Enhanced electrochemical kinetics and polysulfide traps of indium nitride for highly stable lithium-sulfur batteries, ACS Nano 12 (2018) 9578–9586.
[20] Z. Li, Q. He, X. Xu, Y. Zhao, X. Liu, C. Zhou, D. Ai, L. Xia, L. Mai, A 3D Nitrogen-doped graphene/TiN nanowires composite as a strong polysulfide anchor for lithium–sulfur batteries with enhanced rate performance and high areal capacity, Adv. Mater. 30 (2018) 1804089–1804096.
[21] S. Huang, Y.V. Lim, X. Zhang, Y. Wang, Y. Zheng, D. Kong, M. Ding, S.A. Yang, H.Y. Yang, Regulating the polysulfide redox conversion by iron phosphide nanocrystals for high-rate and ultrastable lithium-sulfur battery, Nano Energy 51 (2018) 340–348.
[22] H. Li, S. Ma, H. Cai, H. Zhou, Z. Huang, Z. Hou, J. Wu, W. Yang, H. Yi, C. Fu, Y. Kuang, Ultra-thin Fe_3C nanosheets promote the adsorption and conversion of polysulfides in lithium-sulfur batteries, Energy Storage Mater. 18 (2019) 338–348.
[23] H.C. Chang, T.W. Healy, E. Matijević, Interactions of metal hydrous oxides with chelating agents: III. Adsorption on spherical colloidal hematite particles, J. Colloid Interface Sci. 92 (1983) 469–478.
[24] G. Zhou, E. Paek, G.S. Hwang, A. Manthiram, Long-life Li/polysulphide batteries with high sulphur loading enabled by lightweight three-dimensional nitrogen/sulphur-codoped graphene sponge, Nat. Commun. 6 (2015) 7760–7770.
[25] Z. Lin, X. Li, W. Huang, X. Zhu, Y. Wang, Z. Shan, Active platinum nanoparticles as a bifunctional promoter for lithium – sulfur batteries, ChemElectroChem 4 (2017) 2577–2582.
[26] H. Al Salem, G. Babu, C.V. Rao, L.M.R. Arava, Electrocatalytic polysulfide traps for controlling redox shuttle process of Li-S batteries, J. Am. Chem. Soc. 137 (2015) 11542–11545.
[27] X. Liang, C. Hart, Q. Pang, A. Garsuch, T. Weiss, L.F. Nazar, A highly efficient polysulfide mediator for lithium-sulfur batteries, Nat. Commun. 6 (2015) 5682–5689.
[28] C. Zheng, S. Niu, W. Lv, G. Zhou, J. Li, S. Fan, Y. Deng, Z. Pan, B. Li, F. Kang, Q.H. Yang, Propelling polysulfides transformation for high-rate and long-life lithium–sulfur batteries, Nano Energy 33 (2017) 306–312.
[29] S.B. Yang, L.J. Zhi, K. Tang, X.L. Feng, J. Maier, K. Mullen, Efficient synthesis of heteroatom (N or S)-doped graphene based on ultrathin graphene oxide-porous silica sheets for oxygen reduction reactions, Adv. Funct. Mater. 22 (2012) 3634–3640.
[30] Q. Pang, J. Tang, H. Huang, X. Liang, C. Hart, K.C. Tam, L.F. Nazar, A nitrogen and sulfur dual-doped carbon derived from polyrhodanine@cellulose for advanced lithium–sulfur batteries, Adv. Mater. 27 (2015) 6021–6028.
[31] T. Pan, Z. Li, Q. He, X. Xu, L. He, J. Meng, C. Zhou, Y. Zhao, L. Mai, Uniform zeolitic imidazolate framework coating via in situ recoordination for efficient polysulfide trapping, Energy Storage Mater. (2019).
[32] Z. Chang, Y. He, H. Deng, X. Li, S. Wu, Y. Qiao, P. Wang, H. Zhou, A multifunctional silly-putty nanocomposite spontaneously repairs cathode composite for advanced Li – S batteries, Adv. Funct. Mater. 28 (2018) 1804777–1804786.
[33] T. Zhou, W. Lv, J. Li, G. Zhou, Y. Zhao, S. Fan, B. Liu, B. Li, F. Kang, Q.H. Yang, Twinborn TiO_2–TiN heterostructures enabling smooth trapping–diffusion–conversion of polysulfides towards ultralong life lithium–sulfur batteries, Energy Environ. Sci. 10 (2017) 1694–1703.
[34] Z. Liu, B. Liu, P. Guo, X. Shang, M. Lv, D. Liu, D. He, Enhanced electrochemical kinetics in lithium-sulfur batteries by using carbon nanofibers/manganese dioxide composite as a bifunctional coating on sulfur cathode, Electrochim. Acta 269 (2018) 180–187.
[35] Y. Yang, Z. Wang, T. Jiang, C. Dong, Z. Mao, C. Lu, W. Sun, K. Sun, A heterogenized Ni-doped zeolitic imidazolate framework to guide efficient trapping and catalytic conversion of polysulfides for greatly improved lithium–sulfur batteries, J. Mater. Chem. A 6 (2018) 13593–13598.
[36] C.H. Chang, S.H. Chung, A. Manthiram, Effective stabilization of a high-loading sulfur cathode and a lithium-metal anode in Li-S batteries utilizing SWCNT-modulated separators, Small 12 (2016) 174–179.